Semicrystalline and Superlattice Structures in an Asymmetrically Methyl-Branched Long-Chain Alkane

X. B. Zeng,* F. Xie, and G. Ungar

Department of Engineering Materials, Sheffield University, Sheffield S1 3JD, U.K.

Received May 1, 2007; Revised Manuscript Received June 1, 2007

ABSTRACT: A series of lamellar structures have been found during melt-crystallization of an asymmetrically branched long-chain alkane, $C_{192}H_{385}CH(CH_3)C_{99}H_{199}$, by small- and wide-angle X-ray scattering and DSC. The results show that methyl branches cannot be tolerated in the crystalline layer, consequently two semicrystalline forms are found to crystallize directly from melt depending on the crystallization temperature. In the semicrystalline form crystallized at higher temperatures (HTSCF) the longer arms, i.e., $-C_{192}H_{385}$, form the crystalline layers, while the shorter arms, i.e., $-C_{99}H_{199}$, remain outside as *cilia* to form the amorphous layers. In the semicrystalline form that crystallizes at lower temperatures (LTSCF), the crystalline layers consist of complete short arms and incomplete long arms of the molecules, while the remaining segments of the molecules form the amorphous layers. The HTSCF is thermodynamically stable. HTSCF transforms into a double-layer ABAB superlattice upon further cooling, as the amorphous short arms crystallize and form crystalline B layers. The LTSCF is found to be metastable and transforms into a triple layer ABAABA superlattice upon annealing. The HTSCF and double-layer superlattice have unusually high chain tilt angle (up to 49°). This is the result of excessive steric overcrowding at the crystal−amorphous interface, caused by the disproportionately high number of cilia imposed by the topology which does not allow chain-folding.

1. Introduction

Monodisperse ultralong chain *n*-alkanes C_nH_{2n+1} ($100 \leq n \leq 390$) have been used as model systems in the studies of polymer crystallization ever since their first synthesis in 1985.[1−3] Unlike their polydisperse polymer counterparts, the mature forms of these ultralong chain alkanes have nearly 100% crystallinity. In such lamellar structures the alkane molecules are either extended or folded in 2, 3, ..., *m*, with the folds and chain ends always at the crystal surface. Consequently the lamellar long period is an integer fractions (IF) of the extended chain length L corrected for the chain tilt angle φ.[4] However, IF forms, where molecules fold at least once are always found to crystallize from melt through transient semicrystalline forms. These are termed non-integer fraction (NIF) forms because their lamellar thickness falls between the quantized values of IF forms.[5] Small-angle X-ray scattering analysis has shown that the NIF forms consist of alternating crystalline and amorphous layers.[6] The crystalline layer thickness (l_c) is found to correspond exactly to $(L \cos \varphi)/m$, revealing the fact that crystalline layers consist of integer-folded, fully crystallized molecules, as well as partially crystallized molecules. The latter traverse the crystalline layers less than *m* times, with their tails remaining in the amorphous layers as *cilia*. The fact that fully crystallized molecules in semicrystalline NIF forms are integer-folded with tight chain folds, supports the adjacently reentrant chain folding model of semicrytalline polymers.[7] Due to the fact that the cross-sectional area of an amorphous chain is much larger than that of a straight crystalline chain,[8,9] there is an overcrowding problem at the crystal−amorphous interface.[10] This can only be overcome by the existence of tight chain folds, often assisted by chain tilting. In the NIF forms, the extra cross-sectional area required by the *cilia* is provided by other chains folding back or ending at the crystal surface.

* To whom correspondence should be addressed. E-mail: x.zeng@sheffield.ac.uk.

Semicrystalline forms (SCF) also feature prominently in binary mixtures of long alkanes.[11,12] SCFs are structurally very similar to NIF forms: the shorter molecules are fully crystalline and determine the thickness of the common crystal layer, while the longer molecules are only partially crystalline, their remaining tails forming the amorphous layer. If the shorter chains are extended, the resolution of surface overcrowding is borne entirely by chain ends. While NIF in pure alkanes is always metastable and transforms with time to IF forms, SCFs can be thermodynamically stable due to the entropic effects.[12]

Lamellar structures of long chain alkanes with a methyl or butyl branch in the middle of the chain, $C_{96}H_{193}CH(CH_3)C_{94}H_{189}$ and $C_{96}H_{193}CH(C_4H_9)C_{94}H_{189}$, have been studied.[13−16] It is found that the lamellar thicknesses in both cases correspond to half of the extended molecular chain length, suggesting that the braches are located at the crystal layer surfaces. In comparison, shorter alkanes with central methyl, butyl, hexyl, and butyl phenyl branches respectively were found to crystallize with their branches incorporated in the crystal.[17,18]

In the present paper we describe lamellar structures of the methyl-branched long alkane $C_{192}H_{385}CH(CH_3)C_{99}H_{199}$, where the branch is positioned approximately 1/3 of the way along the chain (Figure 4a). The compound has been synthesized and kindly donated to us by Dr. G. M. Brooke and co-workers of University of Durham.[19] For convenience it will be referred to as the asymmetrically branched alkane. It will be shown in the following that introduction of even such a short branch prevents crystallization in the usual extended or once-folded conformation. Instead unusual semicrystalline and superlattice structures are obtained by melt-crystallization. The results also illustrate the potential for controlling polymer morphology through targeted branching.

2. Experimental Section

Simultaneous small- and wide-angle X-ray scattering (SAXS and WAXS) experiments were carried out at station 16.1 of the Daresbury Synchrotron Radiation Source. Monochromatic beam of

10.1021/ma070992u CCC: $37.00
Published on Web 07/11/2007

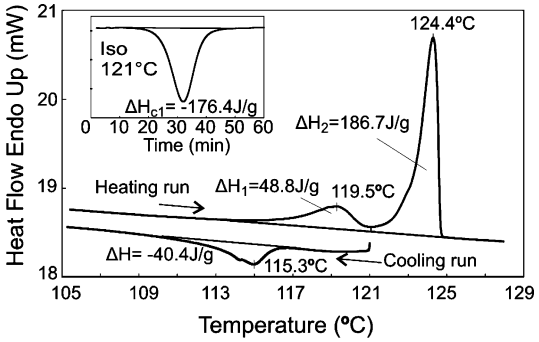

Figure 1. DSC thermograms of the asymmetrically branched alkane recorded during isothermal crystallization at 121 °C (inset) and during subsequent cooling and heating at 0.5 °C/min.

wavelength $\lambda = 1.40$ Å was used. Alkane samples in glass capillaries were held in a modified Linkam hotstage with a precision in temperature control of ±0.1 °C. A quadrant multiwire proportional detector and an Inel 120° curved one-dimensional position-sensitive detector were used for the collection of SAXS and WAXS spectra, respectively. The detector response was corrected using uniform radiation from a ^{55}Fe source. The sample-to-detector distance was calibrated using a series of long chain *n*-alkanes with known lamellar spacings.

From the integrated intensities of discrete small-angle X-ray diffraction peaks, the electron density profile (EDP) normal to the lamellar stacks of the corresponding structure can be reconstructed via Fourier summation, using the general formula

$$E(x) = \sum_{n=1}^{\infty} \sqrt{I_n} \cos\left(\frac{2\pi x}{l} + \phi_n\right) \approx \sum_{n=1}^{N} \sqrt{I_n} \cos\left(\frac{2\pi x}{l} + \phi_n\right) = E_{\exp}(x)$$

where $E(x)$, $E_{\exp}(x)$ are electron density profiles, I_n is the intensity of the *n*th order diffraction peak, l is the long period, and ϕ_n is the phase angle, which is either 0 or π for a centrosymmetric EDP. For more details and examples of the electron density reconstruction procedure see ref 6.

In order to analyze the reconstructed profile $E_{\exp}(x)$ more quantitatively, model electron density profiles $E_{\mathrm{mod}}(x)$ were used to fit the observed diffraction intensities. Since absolute scattering intensities were not determined, electron densities are obtained on a relative scale. For most model profiles used in this work, crystalline layers are assigned one constant density and the intercalated amorphous (surface) layers another constant lower density. Sharp instead of sloping boundaries are used between layers of different densities, in order to simplify the model, even though sloping boundaries normally give a better fit to the experimental data. Fourier expansion of the model profile $E_{\mathrm{mod}}(x)$ was also carried out, yielding the simulated profile $E_{\mathrm{sim}}(x)$. In the construction of $E_{\mathrm{sim}}(x)$ the same number of terms ("diffraction orders") were used as in the reconstruction of $E_{\exp}(x)$. A comparison between $E_{\exp}(x)$ and $E_{\mathrm{sim}}(x)$ thus provides a measure of the goodness of fit of the model, since the truncation effects for the two Fourier expansions are equal.[6] Since the chemical composition is constant throughout the material, the electron density profile is equivalent to the mass density profile.

DSC experiments were carried out on a Perkin-Elmer Pyris-II machine. The temperatures and heats of fusion were calibrated with a standard Indium sample. The phase transition temperatures were determined from the peak values of the heating endotherms, after corrections for both heating rate and the heat resistance between the sample pan and the pan holder (finite value of the slope $d\phi/dT$, where ϕ is the recorded heat flow).[20] Both temperature corrections can be determined from the heating endotherms of standard Indium sample carried out at several different heating rates. The temperature correction for cooling scans was performed by linear extrapolation of the $d\phi/dT$ slope to the appropriate negative heating rate. All peak temperatures given in the DSC thermograms were corrected. For the calculation of crystallinity, the heat of fusion of 100% crystalline polyethylene was taken as 292 J/g.

3. Results

In the asymmetrically branched alkane, two semicrystalline forms were found to form directly from the melt, depending on the crystallization temperature. From these two semicrystalline forms, a double-layer and a triple-layer superlattice structure, respectively, are produced on subsequent solid-state transformation. In the following we will describe these four lamellar structures in turn, on the basis of X-ray scattering and DSC data.

3.1. Melt-Crystallization at Low Supercoolings.

3.1.1. High-T_c Semicrystalline Form (HTSCF). At low supercoolings, in the temperature region between 117.5 and 121.5 °C, the asymmetrically branched alkane is found to crystallize directly from the melt in what we call the high-T_c semicrystalline form (HTSCF). The melting point of HTSCF is determined to be 124.5 ± 0.5 °C by DSC. Crystallization is slow for HTSCF and at 121 °C the crystallization process takes over 40 min to complete, as shown in Figure 1 (inset). The semicrystalline nature of the phase is confirmed by DSC. The measured enthalpy of crystallization at the above temperature is 176 J/g, indicating a crystallinity of only 60%.

The SAXS spectrum of the high-T_c semicrystalline form (Figure 2a, 121 °C) shows four clear peaks, assigned to the first, second, fourth, and fifth diffraction orders from the same lamellar periodicity of $L = 260$ Å. The intensity distribution is typical of that of a semicrystalline structure, where the intensity of the first-order diffraction peak is much higher than those of other orders. The measured intensities of the diffraction peaks are listed in Table 1.

From the intensities, electron density profile $E_{\exp}(x)$ of HTSCF can be reconstructed (solid line, Figure 3). The EDP clearly shows two plateaux in one period, which can be easily attributed to an alternating crystalline−amorphous lamellar structure. The diffraction intensities can be fitted nicely by a model EDP with the shape of a simple rectangular wave function. The best fit model EDP is overlaid on the reconstructed EDP in Figure 3. A simulated reconstruction from the model EDP is also displayed in Figure 3 for comparison. The thicknesses of the crystalline and the amorphous layers, according to the best fit model EDP as shown in Figure 3, are 171 and 89 Å respectively. This corresponds to a volume crystallinity of 0.66 and a crystallinity by weight of 0.69, which is close to that measured from DSC (0.60 measured on isothermal crystallization and 0.64 on heating).

On the basis of the DSC and SAXS results, a structural model of HTSCF is proposed and schematically drawn in Figure 4b. In the model only the longer arm ($-C_{192}H_{385}$) of the molecules is crystallized, forming the crystalline layer. The shorter arm ($-C_{99}H_{199}$) stays outside forming the amorphous layer. Thus, an alternating crystalline−amorphous layered structure is formed. For each molecule, the methyl branch and the end of the long arm are always on the opposite surfaces of the crystalline layer.

3.1.2. Double-Layer Superlattice. SAXS and WAXS spectra recorded simultaneously during cooling of HTSCF are shown in Figure 2. A clear solid-state transition is observed at around 115 °C both in the SAXS spectra (Figure 2a) and in the DSC thermogram (Figure 1), but WAXS diffractograms show only a relatively small change upon this transition. Diffraction peaks up to seventh order of a lamellar structure with spacing 270 Å characterize this new phase (Table 1). There is no evidence of further change in either lamellar spacing or diffraction intensities

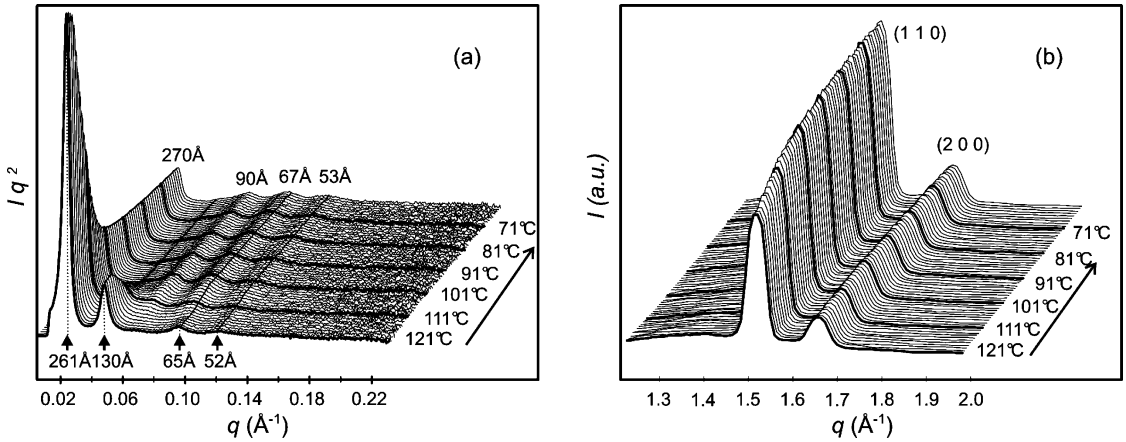

Figure 2. SAXS (a) and WAXS (b) diffractograms of the asymmetrically branched sample recorded simultaneously during a 2 °C/min cooling run from 121 to 61 °C. The sample had been isothermally crystallized at 121 °C for over an hour before the cooling started.

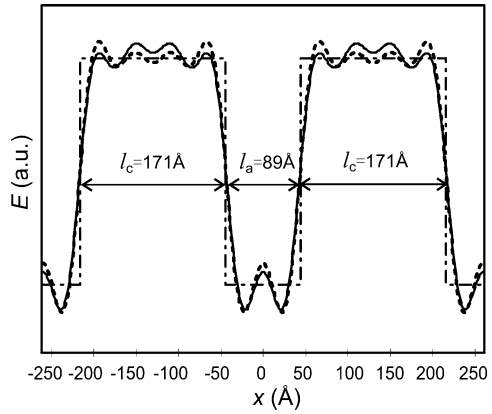

Figure 3. Electron density profiles of HTSCF, covering two full periods. Solid line: profile reconstructed from experimental diffraction intensities ($E_{exp}(x)$); dotted straight line: best fit model ($E_{mod}(x)$); broken line: simulated reconstruction ($E_{sim}(x)$). l_c and l_a are defined in Table 1. The phase angles ϕ_n used in the reconstruction are also listed in Table 1.

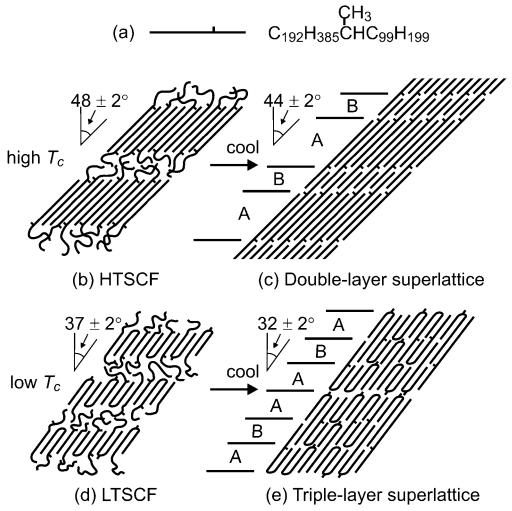

Figure 4. Schematic drawings of various lamellar structures found in the asymmetrically branched alkane: (a) the molecule, (b) high-T_c semicrystalline form, (c) double-layer superlattice, (d) low-T_c semicrystalline form, and (e) triple-layer superlattice.

with continued temperature decrease below 90 °C (Figure 2). Spacings, intensities and chosen phase angles for this phase are given in Table 1. The reconstructed EDP $E_{exp}(x)$ of a repeat period shows two alternating high-density plateaux, one wide and the other narrow, with narrow low-density gaps between them, as shown in Figure 5. This density profile can be explained by crystallization of the amorphous layer of the original HTSCF, which contained the shorter $-C_{99}H_{199}$ arm of the molecules (Figure 4c).

The best fit model EDP ($E_{mod}(x)$, dotted line, Figure 5), assuming constant values for both high and low-density regions, suggests that the thicknesses of the two high-density layers are 177 Å and 27 Å respectively, while the thickness of the low-density gaps is 33 Å. The simulated reconstruction of the model EDP $E_{sim}(x)$ is also shown in Figure 5 for comparison. The thickness of the layers of longer arms ($-C_{192}H_{385}$) hardly changes with the solid-state transition on cooling, while in the middle of the original low-density layers of shorter arms ($-C_{99}H_{199}$), a new crystalline layer appears. It should be noted that the thickness of the new layer in the best fit model, 27 Å, should be treated with caution. The last X-ray diffraction peak recorded is the seventh order, meaning that the resolution limit of the experiment is only ~20 Å. The slight increase of the total lamellar spacing, from 260 Å in HTSCF to 270 Å in the double-layer superlattice, suggests a reduced tilt angle in the crystal layers of the superlattice.

The volume crystallinity of the double-layer superlattice according to the best-fit EDP is 0.76, which converts to 0.78 crystallinity by weight. Despite the uncertainty in determining the thickness of the new crystalline layer, the result fits well with that of DSC (0.74 measured on cooling and 0.81 on heating). Meanwhile, WAXS spectra (Figure 2b) recorded simultaneously during the 2 °C/min cooling run suggest an increase in crystallinity of 18% of the initial value upon the transition from HTSCF to the double-layer superlattice, close to the jump of 23% as observed by DSC. However, on the basis of the ideal structural model shown in Figure 4c, a 50% increase in crystallinity is expected. This suggests that the crystallinity of the newly formed B layers is poorly developed. This could be linked to the fact that the transition involves crystallization of molecular tails, one end of each tail always being confined to the surface of an existing crystalline layer. As a matter of fact, similar behavior has already been observed for binary mixtures, e.g., 50:50 wt % mixture of $C_{162}H_{326}$ and $C_{246}C_{494}$.[11] In the case of the mixtures, the thin middle layer of the triple-layer ABAABA superlattice was shown by Raman spectroscopy to have only part of the cilia contributing to the longitudinal acoustic mode (LAM) vibration near the transition temperature.[21] Hence only part of the chains traversing the middle layer were in their all-trans crystalline conformation, with lowering temperature this fraction increased continuously.

Table 1. Experimental and Calculated Diffraction Intensities of Various Lamellar Phases Observed in Melt-Crystallization of Asymmetrically Branched Long Alkane[a]

phase	*d* spacing, Å	parameters[b]					diffraction intensities											crystallinity		
								1	2	3	4	5	6	7	8	9	*R*	X-ray mass	X-ray vol	DSC
HTSCF	260	l_c/E_c	l_a/E_a				expt	100	17.3	0	4.4	2.7					0.068	0.69	0.66	0.60−0.64
		171 Å/1.0	89 Å/0.85				model	93.1	21.1	0.1	6.3	3.0								
LTSCF	168	l_c/E_c	l_a/E_a				expt	100	2.8	8.4							0.006	0.59	0.55	0.63
		93 Å/1.0	75 Å/0.85				model	99.6	2.8	8.7										
double layer superlattice	270	l_{c1}/E_{c1}	l_{a1}/E_{a1}	l_{c2}/E_{c2}	l_{a2}/E_{a2}		expt	100	6.8	35.5	51.1	40.4	6.9	4.9			0.087	0.78	0.76	0.74−0.75
		177 Å/1.0	33 Å/0.91	27 Å/1.0	33 Å/0.91		model	101.8	5.1	25.5	62.9	37.7	5.8	0.0						
triple layer superlattice	318	l_{c1}/E_{c1}	l_{a1}/E_{a1}	l_{c2}/E_{c2}	l_{a2}/E_{a2}	l_{c3}/E_{c3}	l_{a3}/E_{a3}	expt	0	44.4	100	0	20.7	27.8	0	9.6	5.0	0.080	0.75	0.72	0.74−0.78
		84 Å/1.0	28 Å/0.91	64 Å/0.97	28 Å/0.91	84 Å/1.0	30 Å/0.84	model	0.1	38.5	95.7	0.3	26.6	33.4	0.1	8.3	3.3				

[a] Diffraction intensities are normalized to that of the strongest peak observed. For each phase, the parameters of the best fit model are given. The quality of fit is given by the factor $R = (\sum_n |I_{n,\mathrm{exp}}| - |I_{n,\mathrm{mod}}|)^2/\sum_n |I_{n,\mathrm{exp}}|^2)^{1/2}$. Crystallinities calculated from the models are compared to that measured by DSC. [b] L_c is the thickness of the crystalline layer, and L_a is the thickness of the amorphous or the intercrystalline layer. E_a and E_c are the relative electron densities. In the model it is always assumed that the highest electron density corresponds to that of the perfect crystal, and the lowest electron density to that of amorphous polyethylene.

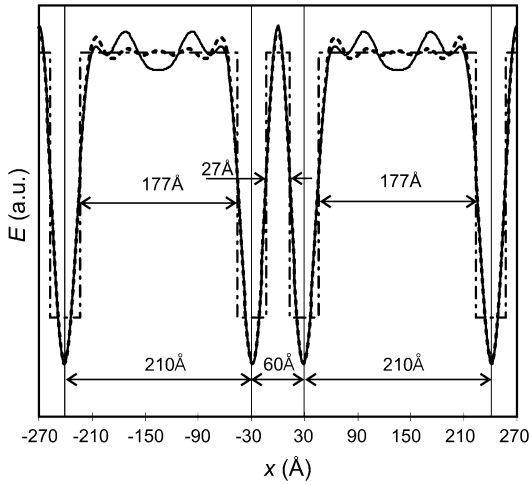

Figure 5. Reconstructed electron density profile of the double-layer superlattice (solid line), best fit model (dot-dash line), and simulated reconstruction (broken wavy line).

The phase transition between the high-T_c semicrystalline form and the double-layer superlattice is reversible. This reversibility, with a relatively small hysteresis, is clearly seen from the heating DSC thermogram recorded subsequent to cooling the HTSCF (Figure 1). Thus, due to the presence of the methyl branch, crystallization of the alkane occurs in two steps: crystallization of the longer $-C_{192}H_{385}$ arm at a higher temperature, and of the shorter $-C_{99}H_{199}$ arms at a lower temperature.

3.2. Melt-Crystallization at High Supercoolings.

3.2.1. Low-T_c Semicrystalline Form (LTSCF). HTSCF forms only at low supercoolings and its crystallization rate is low. At higher supercoolings (below 117 °C, i.e. $\Delta T > 7.5$ °C) or on fast cooling the asymmetrically branched alkane shows a rather different crystallization behavior. Figure 6 shows sequences of SAXS and WAXS spectra recorded simultaneously during isothermal crystallization at 108 °C, i.e., at $\Delta T =$ 16.5 °C. According to the SAXS spectra, at $t = 20-30$ s after reaching T_c, the sample starts to crystallize with a lamellar spacing of 170 Å. In the first several minutes, the diffraction pattern is dominated by the first-order diffraction peak, the intensity of which is much higher than that of other diffraction orders (Table 1). The intensity of the first-order peak rises sharply in the first few frames, reaches a maximum at $t = 1$ min, and then decreases continuously. The long period also decreases continuously, from $l = 170$ Å in frame 3 to $l = 160$ Å at $t = 5$ min. Upon further annealing, a solid-state transformation is clearly observed. A new diffraction peak appears corresponding to ~110 Å, gradually becoming the strongest in the spectrum. Other new diffraction features appear at higher q, also as a result of the solid-state transformation.

Three diffraction orders can be observed for the phase directly formed from the melt. Reconstructed EDP, using SAXS diffraction intensities collected in frame 6 (Figure 6a), is shown in Figure 7 (spacings, intensities and chosen phase angles are given in Table 1). The EDP has two plateaux per period, one high density and the other low density, separated by a sharp boundary. As it signifies alternating crystalline and amorphous layers, such profile is characteristic of a semicrystalline form, which we will refer to as the low-T_c semicrystalline form (LTSCF). The thicknesses of the crystalline and amorphous layers, corresponding to the best fit two-density EDP model, are, respectively, 93 and 75 Å. Thus, volume crystallinity of LTSCF is only 0.55 (0.59 by weight), very close to the value of 0.62 observed in DSC (Figure 8).

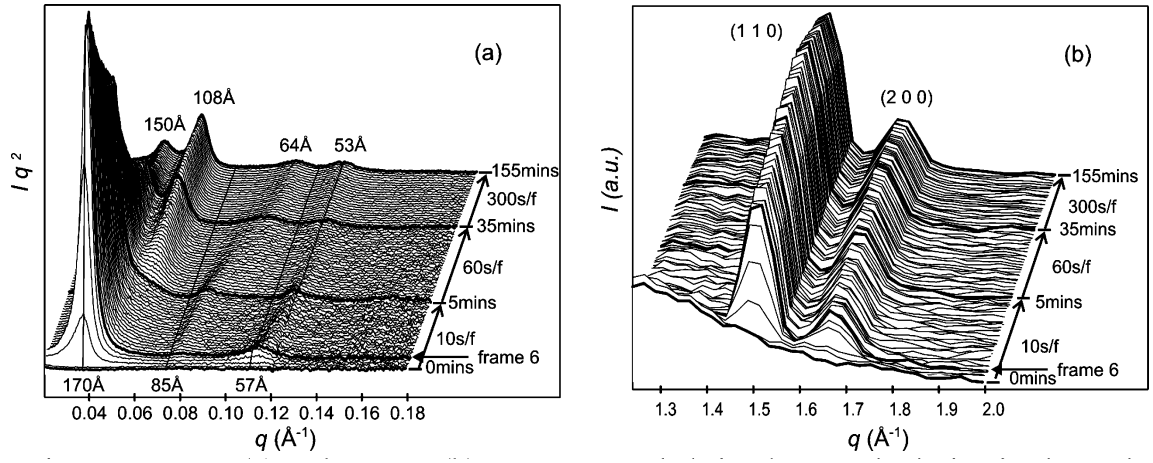

Figure 6. SAXS (a) and WAXS (b) spectra recorded simultaneously during isothermal crystallization of the asymmetrically branched alkane at 108 °C. The first 30 frames were recorded at 10 s intervals, the next 30 frames every 60 s, and the last 24 frames every 300 s.

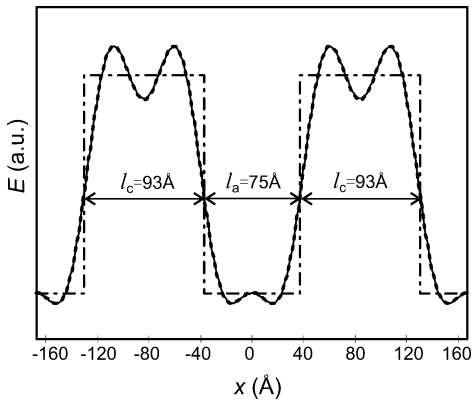

Figure 7. Reconstructed electron density profile of the low-T_c semicrystalline form (solid line), best fit model (dot-dash line) and simulated reconstruction (dotted wavy line). The simulated and experimental EDPs are almost identical.

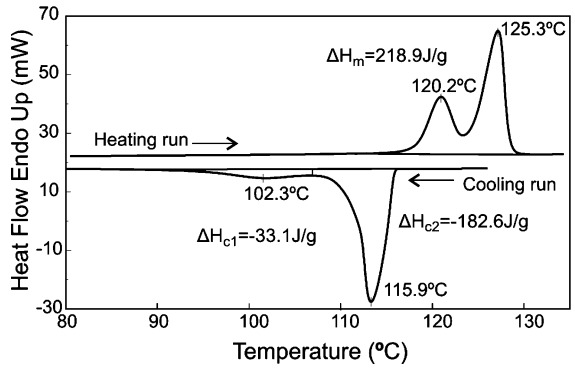

Figure 8. DSC thermogram of the asymmetrically branched alkane recorded during cooling from melt and subsequent heating, both at 10 °C/min. The ΔH_m value on the heating run refers to the combined area of the two endotherms.

The structural model of the low-T_c semicrystalline form, compatible with $E_{mod}(x)$ in Figure 7, is schematically drawn in Figure 4d. As in all other forms, the methyl branches are excluded from the crystalline layers. There are several options for the location of the two arms of a molecule. The shorter arm can be either fully crystalline or fully amorphous. The long arm can traverse the crystal layer only once, with its surplus length contributing to the amorphous layer, or it could be nearly fully crystalline but folded in two, as its length is close to double that of the shorter arm. From the weight crystallinity of LTSCF, it can be roughly estimated that on average one molecule

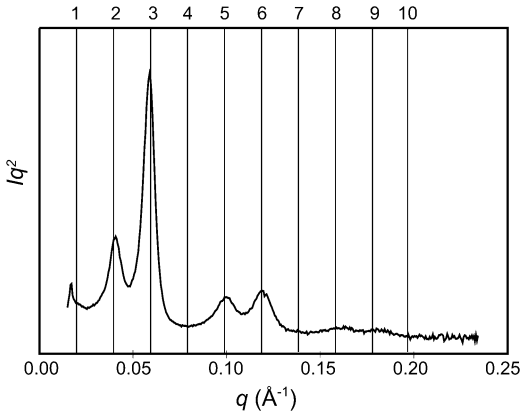

Figure 9. SAXS spectrum of the triple-layer superlattice, after isothermal crystallization at 103 °C and subsequent annealing overnight at the same temperature. The diffraction peaks can be assigned to a 1-d lamellar lattice with a spacing of 318 Å. Vertical lines indicate the expected positions of diffraction orders.

traverses the crystalline layer twice, with its remaining part in the amorphous layer.

3.2.2. Triple Layer Superlattice. Upon further annealing or cooling, LTSCF gradually transforms to another phase. The phase transition is clearly evident from both SAXS spectra (Figure 6a) and from the DSC (Figure 8). The best quality SAXS spectra of this phase are observed after annealing at high temperatures (Figure 9, sample annealed overnight at 103 °C). Six diffraction peaks can be clearly identified, and they can be attributed to the second, third, fifth, sixth, eighth, and ninth orders of a lamellar structure with a period of 318 Å.

The density profile of this new phase, reconstructed from the diffraction intensities, suggests that the phase has an ABA type triple-layer superlattice structure (Figure 10)., There are three high-density plateaux within one period, the middle one having a slightly lower density than the other two—see Figure 10. Between the high-density layers there are narrow low-density gaps. The gap between the two highest plateaux is almost twice as deep as the other two gaps in the same period. In the best fit EDP model $E_{mod}(x)$ (dot-dash line), the thicknesses of the A and B crystalline layers are 84 and 64 Å, respectively. The width of the gaps between AA layers is 30 Å, while that between AB layers is 28 Å (note: the resolution limit of the SAXS experiment is ~20 Å). The best fit EDP model suggests a volume crystallinity of 0.72 and a weight crystallinity of 0.75. Again, this is close to the value of 0.74 determined by DSC (Figure 8). The evolution of integrated WAXS intensity

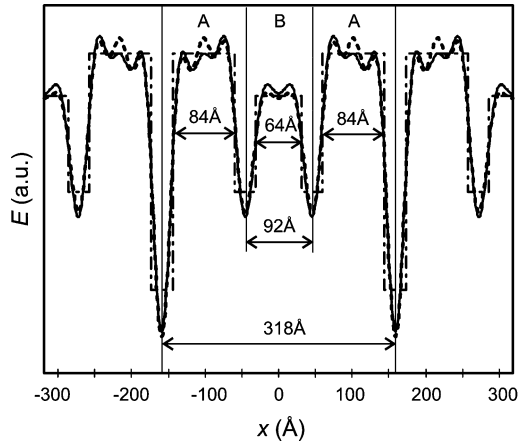

Figure 10. Reconstructed electron density profile of the triple-layer superlattice (solid line), best fit model (dotted straight line) and simulated reconstruction (broken wavy line).

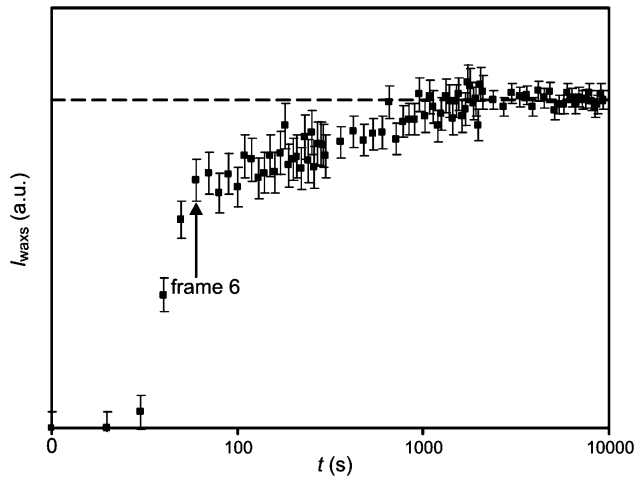

Figure 11. Evolution of integrated WAXS intensity $I_{waxs} = I_{110} + I_{200}$ with time during isothermal crystallization of the asymmetrically branch alkane at 108 °C.

$I_{waxs} = I_{110} + I_{200}$ with time during isothermal crystallization at 108 °C is shown in Figure 11. In line with the SAXS and DSC results, it shows the initial crystallization in the LTSCF form, and its subsequent transition to triple-layer superlattice. After ~30 min, I_{waxs} reached a plateau for the triple-layer superlattice, the crystallinity of which is increased by 30% compared to that of LTSCF in frame 6. This is in good agreement with the 27% increase in crystallinity suggested by the EDP models.

On the basis of the reconstructed EDP, a structural model is proposed as schematically drawn in Figure 4e. We suggest that, in this ABA triple-layer superlattice, the A layers are formed already during the initial crystallization of the semicrystalline form, while the B layers in the middle form later during the solid-state transition. The transition can be viewed as secondary crystallization in every other initially amorphous layer. While one B layer is intercalated between two A layers in this process, the *cilia* on the other side of the A layers are depleted in order to feed the B layer. Consistent with the density profile (Figure 10), in such a triple layer superlattice, every third intercrystalline layer (A−A gap) is believed to be devoid of cilia and tie-molecules crossing the gap, thus making the density gap deeper. In contrast, A−B gaps contain a sizable fraction of tie molecules. The structural model explains satisfactorily the reconstructed EDP, and is consistent with molecular dimensions. The transition between the LTSCF and the triple-layer superlattice is similar to that between the semicrystalline form (SCF)

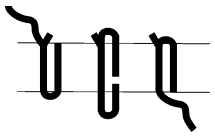

Figure 12. Suggested "cilium flip" process transferring the cilium from one side of the crystalline A layer to the other in the LTSCF → triple layer transition (Figure 4d → Figure 4e).

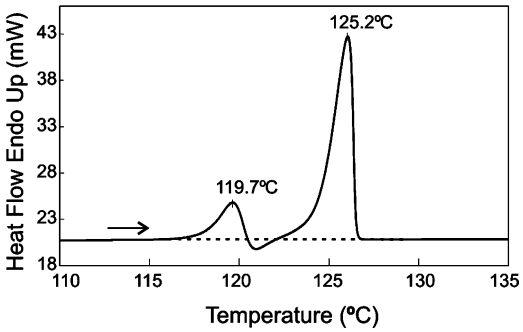

Figure 13. DSC thermogram of asymmetrically branched alkane on heating from the triple-layer superlattice to the melt. Heating rate is 2 °C/min. Unlike in the 10 °C/min heating run in Figure 9, melting of the triple layer superlattice and recrystallization of HTSCF can be clearly resolved.

and the low-temperature triple-layer superlattice observed in binary mixtures of linear long alkanes.[12] However, while in the binary mixtures cilium transfer from one side of the crystalline A layer to the other can proceed through simple chain translation ("sliding diffusion"), the equivalent cilium flip in the branched alkane may also require processes such as that depicted in Figure 12, if pulling the methyl branch through the crystal is to be avoided.

Unlike the transition between the HTSCF and the double-layer superlattice, described in the preceding section, the solid-state transition between the LTSCF and the triple-layer superlattice is irreversible. Once the triple-layer superlattice is formed, on subsequent heating it transforms to the HTSCF, bypassing the metastable LTSCF. The triple-layer to HTSCF transformation proceeds through melting and recrystallization, as evidenced by the exotherm in the slow-heating DSC thermogram in Figure 13. Melting of the triple-layer phase appears to be a one-step process, i.e., both A and B layers melt simultaneously. This is attributed to their similar thicknesses.

4. Discussion

4.1. Effect of Methyl Branch on the Crystallization Behavior of Long Alkanes. Previous studies on linear long alkanes have established the fact that they always crystallize with their fold length an integer fraction of their total chain length.[3,4] The experimental results presented above, however, show that by introducing a methyl branch in an otherwise linear long alkane, the crystallization behavior of the alkane is drastically altered. The results lead to the conclusion that the methyl branch, small as it is, cannot be tolerated in the crystalline layers. This and the surface overcrowding effect at the crystalline−amorphous interface are the key factors that control the achievable lamellar structures in the asymmetrically branched alkane.

Contrary to the present results showing that methyl branches are rejected from the crystal, in random ethylene−propylene copolymers it was found that up to ca. 7 CH_3 per 100 C atoms can be incorporated into the crystal, causing large expansion of the *a* lattice parameter and even reaching hexagonal symmetry in the limiting case.[22−24] In the current asymmetrically methyl-

branched alkane there is no indication of any significant lattice expansion from WAXS data (within the experimental error of ±0.03 Å), confirming that the methyl branches do not reside in the crystal. A similar result has also been obtained for the symmetrically methyl-branched alkane $C_{96}H_{193}CH(CH_3)C_{94}H_{189}$,[13] and butyl branched alkane $C_{96}H_{193}CH(C_4H_9)C_{94}H_{189}$.[15] Similarly in short-chain methyl-branched alkanes the methyl groups line up in layers, making the conformation and crystal structure different compared to that of the non-branched alkane.[17,18] It can thus be concluded that a sizable number of methyl branches can only be incorporated in the crystal if they are evenly distributed through the crystal volume, but not when they aggregate and strongly interact within a plane.

Unlike the low-T_c semicrystalline form (LTSCF), HTSCF is thermodynamically stable, despite its semicrystallinity. This structure is similar to that in diblock copolymers, where either only one block is capable of crystallization[25] or the temperature is in the region between the melting points of the two blocks when both blocks are crystallizable.[26] However, in block copolymers the chemical compositions of the two blocks are different, and the microphase separation between the two blocks is the driving force for the alternating layered structure. In the asymmetrically branched alkane the two arms are chemically identical, differing only in length, and their separation into different layers in HTSCF is physical in nature.

In comparison, Cheng and co-workers have studied 2-, 3-, and 4-arm branched oligomer fractions where the PEO arms were connected via a benzene ring. The 2-arm PEOs could crystallize in both extended and once-folded conformation, even though the extended conformation became increasingly difficult to achieve as the coupling angle between the arms was changed from 180° (1,4-substitution) to 60° (1,2-substitution).[27−30]

4.2. Chain Tilt and Surface Overcrowding. In melt-crystallized long chain *n*-alkanes and polyethylene the molecular chains are often inclined relative to the lamellar normal, and the most commonly observed tilt angle is 35°, i.e. the fold surface or end-surface is a {201} basal plane of the polyethylene sublattice. It is generally accepted that chain tilting is there to alleviate the overcrowding problem at the crystalline−amorphous interface, where the cross-sectional area of a chain is calculated to expand by a factor between 2 and 3 on entering the amorphous layer from the crystalline layer.[8−10] Our own estimate from phase diagrams of binary long alkanes gave a factor of $f_{exp} = 2.8$ for an end-surface normal to the crystalline chains.[11] The overcrowding problem is solved by a combination of tight chain folding at the crystalline layer surface and chain tilting. In alkanes, the tilt angle can be determined by SAXS by comparing the crystalline layer thickness with the straight molecular chain length.

The contour length of the asymmetrically branched alkane (from the end of the long arm to the end of the short arm) can be calculated as 374 Å. As the observed long period of HTSCF is only 260 Å, the crystallized molecular chains must be inclined to the lamellar surface normal. After correction for different densities of the crystalline and amorphous phases (1.0×10^3 and 0.85×10^3 kg/m^3, respectively), the tilt angle is calculated as 49°, close to that corresponding to the basal plane {301} (ideal crystallographic angle 46°). Similarly, from the best fit model value of crystal layer thickness $l_c = 171$ Å (Figure 3), and the calculated contour length of the long arm (246 Å), we obtain the tilt angle of 46°. However, our studies of alkane mixtures by a combination of X-ray and neutron scattering on end-labeled alkanes[11,31] have shown that the crystalline stem length obtained from the electron density l_c parameter is somewhat less than the actual stem length, due to a disordered layer underneath the crystal surface. Thus, we consider the value of 49° for the tilt angle in HTSCF as the more credible one. We note that, although the most commonly observed tilt angle in melt-crystallized long chain *n*-alkanes and polyethylene is 35°, tilt angles larger than 45° have been observed in polyethylene in exceptional cases.[32]

A larger tilt angle is in fact expected for HTSCF phase of the present branched compound, as the surface anchoring of methyl branches forces 50% of the crystalline chains to enter the amorphous layer. This is a higher fraction than in any pure or mixed alkane previously studied. Presumably this fraction is also larger than in polyethylene under normal circumstances, although determining the folded fraction in polyethylene is not a straightforward task. The 0.50 fraction of chains emanating from the crystalline layer of HTSCF, is considerably higher than the "allowed" fraction $1/f_{exp} = 1/2.8 = 0.36$. A 35° chain tilt would allow a somewhat higher fraction of $1/(f_{exp}\cos 35°) = 0.44$ of chains to exit the crystal. Since in HTSCF chain folding is not available to relieve the overcrowding, a higher chain tilt angle becomes the only solution. The measured tilt angle of 49° allows a cilia fraction as high as $1/(f_{exp}\cos 49°) = 0.54$, sufficient to sustain the required topology. Thus, the current experimental data add support to the previously determined f_{exp} value of 2.8. Steric overcrowding may be further exacerbated here by the volume of the methyl branches at the interface, although the effect is localized. This may explain the tilt angle of 49°, slightly higher than necessary solely for the accommodation of the 0.50 cilia fraction.

For LTSCF (Figure 4d), the thickness of the crystalline layer is believed to be determined by the once-folded longer arm (246/2 = 123 Å), which is very close in length to the shorter arm of the molecule (126 Å). As the best fit value for the thickness of the crystalline layer in LTSCF is 93 Å (Figure 8), the calculated chain tilt angle in this layer would be 41°, neglecting the effect of surface layer disorder mentioned above. Taking of the surface disorder into account, the tilt angle would be closer to the 35° as normally observed for linear and branched long alkanes previously studied.[6,13] Because of the variety of conformations that molecules can adopt in LTSCF (Figure 4d), it is not possible to determine the degree of surface overcrowding. However, assuming that all chain folds were ***tight***, the cilia fraction can be estimated as 0.35, which is much less than that in the HTSCF case (0.50). Again, the steric effect of methyl branches may raise the effective overcrowding, making the 35° tilt angle nearly ideal for the topology of LTSCF.

In the double-layer superlattice (Figure 4c), a high tilt angle, similar to that in HTSCF, is observed. From both the lamellar thickness and the crystalline layer thickness in the A layers, the tilt angle is calculated as be 44°. However, for the triple-layer superlattice, the overall long period is 318 Å, suggesting a tilt angle of only 32° according to the structural model (Figure 4e). This can again be attributed to the less severe overcrowding on the crystalline layer surface which allows tight chain folding.

4.3. Disorder in the Intercrystalline Layers. As to the structure of the intercrystalline layers in the double- and triple-layer superlattices, the width of the corresponding density gaps (~30 Å, Table 1) suggests that these layers are more disordered than either in linear (e.g., extended-chain $C_{194}H_{390}$)[6] or centrally methyl-branched long-chain alkane ($C_{96}H_{193}CH(CH_3)C_{94}H_{189}$), in which the gaps are all thinner than 20 Å.[13] Supporting this suggestion are Raman scattering results on the triple-layer superlattice in a 1:1 mixture of linear alkanes $C_{246}H_{494}$ and $C_{162}H_{326}$; these have shown that the LAM vibration of the chains

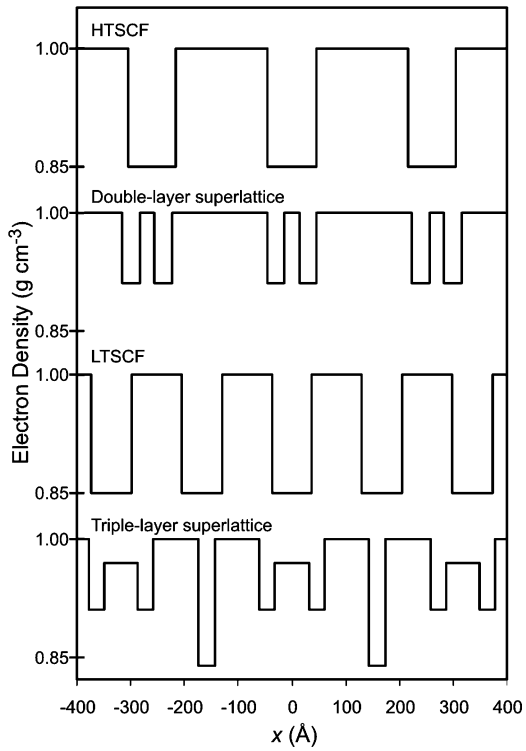

Figure 14. Electron density profiles of different lamellar phases found in the asymmetrically branched alkane.

crossing the intercrystalline gap (the tie-molecule) is decoupled at the gap.[12] Since in the superlattices of the asymmetrically branched alkane the intercrystalline layers also contain methyl branches and, in the triple-layer superlattice also chain folds, it is unlikely that they are any more ordered than the gap layers in mixed linear alkanes, which contain only tie-molecules and chain ends.

As mentioned, the reconstructed electron densities are only on a relative scale. However, as both HTSCF and LTSCF have thick and well-defined crystalline and amorphous layers, their density values can be used as internal standard for electron densities of the superlattices observed in the same temperature run with the sample under identical diffraction geometry. In Figure 14, the best-fit density profiles of all four phases are plotted together on the same density scale. Taking the highest level as the reference crystalline density, it is evident that the density of the intercrystalline layers of the double-layer superlattice is significantly higher than that of the pure amorphous layer. The same is true for the A−B gaps of the triple layer superlattice. At the same time, the density of the A−A gaps in the triple layer is almost the same as that of the pure amorphous layer. This difference can be explained by the existence of tie molecules in A−B gaps in both double- and triple-layer superlattices. Similarly, an increased gap density due to tie molecules has been found previously in the triple layer superlattice in binary mixtures of long alkanes.[33]

4.4. Melting Temperatures. It is interesting to examine the temperatures of the phase transitions observed in the present asymmetrically branched alkane. The melting point of the high-T_c semicrystalline form is found to be 124.5 ± 0.5 °C. This is somewhat lower than the melting point (126.9 ± 0.3 °C)[34] of the pure alkane $C_{194}H_{390}$, which has a comparable crystalline stem length. The 2.4 °C difference may be explained by the facts that, while the molar melting enthalpy is the same in both cases, the entropy gain per molecule is slightly higher for the branched alkane, due to the longer overall length of the molecules (entropy of the decouple is proportional to ln n, where n is the number of segments in the molecule).[35] The excessive overcrowding of the crystal−amorphous interface in this case, which is only partially relieved by the unusually high chain tilt, may also attribute to lowering the melting point, as the surface free energy σ_e is in this case expected to be higher than usual.

The temperature of the transition between the double-layer superlattice and the high-T_c semicrystalline form is 119.6 ± 0.5 °C, as determined by DSC. This transition corresponds to the melting and recrystallization of the $-C_{99}H_{199}$ arms, i.e., of the B layers in Figure 4. In comparison, the melting points of linear alkanes $C_{94}H_{190}$,[36] $C_{98}H_{198}$,[37] and $C_{102}H_{206}$ are, respectively, 113.5, 115.0, and 115.7 (±0.3) °C.[4] This increased melting temperature of the B layers in the AB superlattice, relative to that of crystals of a free alkane of equivalent length, is in line with expectations. Since after melting one end of the cilium remains pinned to the surface of the crystalline B layer, its entropy is reduced relative to that of a free molten chain, essentially as in the case of a dense polymer brush.[38] This increased melting point is recorded in spite of the crystallinity of the B layer being lower than the crystallinity of linear alkanes, as determined from both SAXS and DSC.

Turning to the triple-layer superlattice, its DSC melting point is 120.0 ± 0.5 °C. This is very close to the melting point of the twice-folded form of the linear alkane $C_{294}H_{590}$ (119.3 ± 0.5 °C).[39,40] Such similarity is expected as both the thickness of the crystalline layers and the molecular masses of the two alkanes are almost equal. It is well established[41] that the melting point of folded chains is higher than that of extended chains of the same crystalline stem length (compare again with T_m = 115.0 °C for $C_{98}H_{198}$).

5. Conclusions

1. Four different lamellar forms were found in the asymmetrically branched alkane.

2. The structures of these lamellar forms were determined by reconstruction of their electron density profiles from the discrete small-angle reflections. The structural models are in good agreement with the DSC results.

3. The two phases found below the melting point are semicrystalline, one of which is thermodynamically stable. Their crystal layer thickness is determined by the length of the long or the short arm of the alkane, respectively.

4. At lower temperatures these phases transform into a double-layer ABAB or a triple layer ABAABA superlattice form, respectively, through rearrangement and crystallization of the amorphous layers.

5. The high-T_c semicrystalline form (HTSCF) and the double-layer superlattice have unusually high chain tilt angle of up to 49°. This is the result of excessive steric overcrowding at the crystal−amorphous interface, caused primarily by the excessive fraction of chains (0.5) crossing the crystalline−amorphous interface.

6. The results suggest that the methyl branches, although small, cannot be tolerated in the crystalline layers of a uniform alkane, as they would aggregate in a single atomic plane. In contrast, when methyls are randomly distributed as in random ethylene−propylene copolymers, a significant concentration of branches is tolerated by a distorted crystal lattice. The coalescence of branches at the layer surface makes crystallization and morphology of the methyl branched alkane profoundly different from those of linear alkanes.

7. The results demonstrate how semicrystalline forms can be induced or even stabilized by targeted introduction of a methyl

branch along a molecular chain, and how complex superlattice structures can be created on subsequent solid-state transformation. In addition, the asymmetrically branched alkane provides an excellent model for examining steric overcrowding at the crystalline−amorphous interface, the problem at the heart of chain folding and polymer morphology.

Acknowledgment. Our special thanks are to Dr. G.M. Brooke and his co-workers at Durham University for the synthesis of the branched alkane. We are also grateful to Mr. A. Gleeson at SRS, Daresbury, U.K., for help with X-ray experiments. F.X. wishes to thank EPSRC for his PhD studentship.

References and Notes

(1) Bidd, I.; Whiting, M. C. *J. Chem. Soc., Chem. Commun.* **1985**, 543−544.
(2) Bidd, I.; Holdup, D. W.; Whiting, M. C. *J. Chem. Soc., Perkin Trans.* **1987**, *1*, 2455−2463.
(3) Lee, K. S.; Wegner, G. *Makromol. Chem., Rapid Commun.* **1985**, *6*, 203−208.
(4) Ungar, G.; Stejny, J.; Keller, A.; Bidd, I.; Whiting, M. C. *Science* **1985**, *229*, 386−389.
(5) Ungar, G.; Keller, A. *Polymer* **1986**, *27*, 1835−1844.
(6) Zeng, X. B.; Ungar, G. *Polymer* **1998**, *19*, 4523−4533.
(7) Frank, F. C. *Discuss. Faraday Soc.* **1979**, *68*, 7−13.
(8) DiMarzio, E. A.; Guttman, C. M. *Polymer* **1980**, *21*, 733−744.
(9) Guttman, C. M.; DiMarzio, E. A.; Hoffman, J. D. *Polymer* **1981**, *22*, 1466−1479.
(10) Gautam, S.; Balijepalli, S.; Rutledge, G. C. *Macromolecules* **2000**, *33*, 9136−9145.
(11) Zeng, X. B.; Ungar, G. *Macromolecules* **2001**, *34*, 6945−6954.
(12) Zeng, X. B.; Ungar, G. *Phys. Rev. Lett.* **2001**, *86*, 4875−4878.
(13) Ungar, G.; Zeng, X. B.; Brooke, G. M.; Mohammed, S. *Macromolecules* **1998**, *31*, 1875−1879.
(14) Hosier, I. L.; Bassett, D. C. *Polymer* **2002**, *43*, 5959−5967.
(15) Rastogi, A.; Hobbs, J. K.; Rastogi, S. *Macromolecules* **2002**, *35*, 5861−5868.
(16) Klein, P. G.; Driver, M. A. N. *Macromolecules* **2002**, *35*, 6598−6612.
(17) Yamamoto, H.; Nemoto, N.; Tashiro, K. *J. Phys. Chem. B* **2004**, *108*, 5827−5835.
(18) Ikedou, K.; Yamamoto, H.; Nagashima, H.; Nemoto, N.; Tashiro, K. *J. Phys. Chem. B* **2005**, *109*, 10668−10675.
(19) Brooke, G. M.; Farren, C.; Harden, A.; Whiting, M. C. *Polymer* **2001**, *42*, 2777−2784.
(20) O'Neil, M. J. *Anal. Chem.* **1964**, *36*, 1238. Höhne, G. W. H. *Differential scanning calorimetry: an introduction to practitioners*; Springer: Berlin and London, 1996.
(21) Zeng, X. B.; Ungar, G.; Spells, S. J. *Polymer* **2000**, *41*, 8775−8780.
(22) Ungar, G.; Keller, A. *Polymer* **1980**, *21*, 1273−1287.
(23) Starkweather, W. H., Jr.; Van Catledge, A. F.; MacDonald, N. R. *Macromolecules* **1982**, *15*, 1600−1604.
(24) Ballesteros, O, R.; Auriemma, F.; Guerra, G.; Corradini, P. *Macromolecules* **1996**, *29*, 7141−7148.
(25) Hamley, I. W. *The physics of block copolymers*, 1998, Oxford University Press: Oxford, U.K., 1998.
(26) Sun, L.; Liu, Y. X.; Zhu, L.; Hsiao, B. S.; Carlos, A.; Avila-Orta, C. A. *Polymer* **2004**, *45*, 8181−8193.
(27) Lee, S.-W.; Chen, E.-Q.; Zhang, A.; Yoon, Y.; Moon, B.-S.; Lee, S.; Harris, F. W.; Cheng, S. Z. D.; von Meerwall, E. D.; Hsiao, B. S.; Verma, R.; Lando, J. B. *Macromolecules* **1996**, *29*, 8816−8823.
(28) Chen, E.-Q.; Lee, S.-W.; Zhang, A.; Moon, B.-S.; Honigfort, P. S.; Mann, I.; Lin, H.-M.; Harris, F. W.; Cheng, S. Z. D.; Hsiao, B. S.; Yeh, F. *Polymer* **1999**, *40*, 4543−4551.
(29) Chen, E.-Q.; Lee, S.-W.; Zhang, A.; Moon, B.-S.; Mann, I.; Harris, F. W.; Cheng, S. Z. D.; Hsiao, B. S.; Yeh, F.; von Meerwall, E. D. In *Scattering from Polymers*; ACS Symposium Series 739: American Chemical Society: Washington, DC, 2000; pp 118−139.
(30) Chen, E. -Q.; Lee, S. -W.; Zhang, A.; Moon, B. -S.; Mann, I.; Harris, F. W.; Cheng, S. Z. D.; Hsiao, B. S.; Yeh, F.; von Meerwall, E. D.; Grubb, D. T. *Macromolecules* **1999**, *32*, 4784−4793.
(31) Zeng, X. B.; Ungar, G.; Spells, S. J.; Brooke, G. M.; Farren, C.; Harden, A. *Phys. Rev. Lett.* **2003**, *90*, 155508.
(32) Varnell, W. D.; Ryba, E.; Harrison, J. R. *J. Macromol. Sci., Phys. B* **1987**, *26*, 135−143.
(33) Zeng, X. B.; Ungar, G. *Polymer* **2002**, *43*, 1657−1666. Zeng, X. B.; Ungar, G. *Macromolecules* **2003**, *36*, 4686−4688.
(34) Boda, E.; Ungar, G.; Brooke, G. M.; Burnett, S.; Mohammed, S.; Proctor, D.; Whiting, M. C. *Macromolecules* **1997**, *30*, 4674−4678.
(35) Flory, P. J.; Vrij, A. *J. Am. Chem. Soc.* **1963**, *85*, 3548−3553.
(36) Hoffman, J. D. *Macromolecules* **1985**, *18*, 772−786.
(37) Teckoe, J.; Bassett, D. C. *Polymer* **2000**, *41*, 1953−1957.
(38) Lai, P. Y.; Binder, K. *J. Chem. Phys.* **1992**, *97*, 586−595.
(39) Ungar, G. Unpublished data.
(40) Sanz, N.; Hobbs, J. K.; Miles, M. J. *Langmuir* **2004**, *20*, 5989−5997.
(41) Buckley, C. P.; Kovacs, A. J. *Prog. Colloid Polym. Sci.* **1975**, *58*, 44−60.

MA070992U